Heat transfer and chemical reaction models for reduction of iron oxide pellets in countercurrent moving bed reactors

Article *in* Steel Research · December 1998

DOI: 10.1002/srin.199805582

CITATION
1

READS
42

3 authors:

Pedro Garnica
Instituto Tecnológico de Morelia (ITM)
37 PUBLICATIONS **86** CITATIONS

SEE PROFILE

Rodolfo D Morales
Instituto Politécnico Nacional
197 PUBLICATIONS **2,393** CITATIONS

SEE PROFILE

Miguel Toledo
Instituto Politécnico Nacional
10 PUBLICATIONS **54** CITATIONS

SEE PROFILE

Heat transfer and chemical reaction models for reduction of iron oxide pellets in countercurrent moving bed reactors

P. Garnica-González, Rodolfo D. Morales and Miguel V. Toledo

Mass, energy and pressure balances are performed in a volume slice of a HyL III reactor in order to build a mathematical simulator for the different reduction steps. Three iron ore feed mixtures were simulated finding, in general, good agreement between plant data for metallization of DRI and the corresponding mathematical simulations. The main differences between these two types of data are explained as a consequence of the low efficiency of the contact between the reducing gases, H_2 and CO, and the bed of solids due to the formation of clusters in the different ore feeds. This tendency observes a remarkable increase with rise of the total iron content in the ore feed. The existence of clusters promotes fluid flow malfunctions affecting the uniformity of the DRI quality expressed as it final metallization. This leads to the need of a 3D simulator which should be able to quantify this effect.
Finally it was found, in the present research, that carbon monoxide plays a minor role in the dynamic behaviour of the reduction for the feed mixtures analyzed with the mathematical simulator.

Wärmeübergangs- und chemische Reaktionsmodelle der Reduktion von Eisenerzpellets in Gegenstromreaktoren. Um die verschiedenen Reduktionsschritte mathematisch simulieren zu können, wurden die Massen-, Energie- und Druckbilanzen in einem Volumenelement eines HyL-III-Reaktors betrachtet. Drei Erzaufgabemischungen wurden simuliert. Im Allgemeinen zeigten die so ermittelten Werte gute Übereinstimmung mit Betriebsdaten, wie z.B. dem Metallisationsgrad. Die gravierenden Unterschiede zwischen beiden Datengruppen beruhen auf der geringen Durchgasung des Feststoffbettes mit den Reduktionsgasen H_2 und CO aufgrund von Clusterbildung in den jeweiligen Erzmischungen. Diese Tendenz wird mit zunehmendem Fe_{tot}-Gehalt in der Erzmischung deutlich verstärkt. Das Vorhandensein von Clustern begünstigt Strömungsfehler, die eine gleichmäßige DRI-Qualität -ausgedrückt durch den Endmetallisationsgrad- beeinträchtigen. Mit einer dreidimensionalen Simulation könnte dieser Effekt quantifiziert werden.
Schließlich führte die vorliegende Untersuchung für die analysierten Aufgabemischungen zu dem Ergebnis, daß Kohlenmonoxid für das dynamische Reduktionsverhalten eine untergeordnete Rolle spielt.

There have been various reports on mathematical models for iron ore reduction in moving bed reactors, specifically, some of them deal with the chemical reactions assuming a three-interface model for transformations of hematite (h) to magnetite (m), magnetite (m) to wustite (w) and wustite (w) to iron (Fe).

Yanagiya et al. [1] applied the chemical reaction model of Hara et al. [2] to this line in order to explain their experimental results in a laboratory moving bed reactor. In both works of research the temperature profile along the reactor axial position was experimentally measured and these data were fed to the chemical reaction model to obtain the gas composition, % of reduction for every reduction step, total reduction and pressure behaviour along the reactor length as outputs. In regard to the coupling of heat transfer with chemical reaction there are the works of Kaneko et al. [3] and Takahashi et al. [4] who explained in this way their experimental results for iron ore reduction in shaft furnaces.

On the other hand, the present authors [5] reported results of a HyL III moving bed, iron ore reduction plant for three-feed mixtures and they were explained by a qualitative basis using a model for a single pellet. In the present work heat transfer and chemical reaction models are coupled in order to explain, on a more quantitative way, those results using the Hara's model for the chemical reaction and employing a different numerical approach to those reported by Kaneko et al. and Takahashi et al. due to the very high stiffness of the resultant system of differential equations.

P. Garnica-González, PhD student; *Professor Dr. Eng. Rodolfo D. Morales*, Department of Metallurgy, Instituto Politécnico Nacional-E.S.I.Q.I.E.; *Professor Dr. Eng. Miguel V. Toledo*, Laboratory of Thermofluids, Instituto Politécnico Nacional-E.S.I.M.E., México.

Mathematical model

Chemical and heat transfer models. As a first approximation to describe the axial distribution of concentrations for H_2, H_2O, CO and CO_2 and the fractional reduction of solids, a one-dimensional mathematical model was derived within the framework of the following assumptions:

- steady state conditions under plug flows of gas and solid,
- uniform temperature within the solid particles,
- three-interface model for representing the overall reduction of the pellet,
- uniform solid voidage throughout the reactor.

The chemical reactions for the three interface model are expressed as:

$$3Fe_2O_3 + H_2 = 2Fe_3O_4 + H_2O, \quad (1)$$

$$Fe_3O_4 + H_2 = 3FeO + H_2O, \quad (2)$$

$$FeO + H_2 = Fe + H_2O, \quad (3)$$

$$3Fe_2O_3 + CO = 2Fe_3O_4 + CO_2, \quad (4)$$

$$Fe_3O_4 + CO = 3FeO + CO_2, \quad (5)$$

$$FeO + CO = Fe + CO_2. \quad (6)$$

Considering a volume slice of the reactor as it is shown in **figure 1** and on the basis of these assumptions the governing equations may be written as follows:

- mass balance of the solid particles, for list of symbols see **table 1**:

$$\frac{dR_i^j}{dz} = \frac{6(1-\varepsilon)}{\pi d_p^3}\frac{S}{W d_{0i}} v_i^j, \qquad (7)$$

where the subscript i stands for magnetite, wustite and iron and the superscript j corresponds to H_2 and CO;

- mass balance of the gas:

$$\frac{dY_i^j}{dz} = \frac{6(1-\varepsilon)}{\pi d_p^3 G} v_i^j; \qquad (8)$$

- total mass balance of reducing gases (H_2 and CO):

$$\frac{dY}{dz} = \frac{6(1-\varepsilon)}{\pi d_p^3}\frac{S}{G}\Sigma v_i^j, \qquad (9)$$

where $Y = Y_i^{H_2} + Y_i^{CO}$, the molar fractions of H_2O and CO_2 at every space step, dz, were calculated using the stoichiometry of reactions (1) - (6) once that the corresponding molar fractions of H_2 and CO were known.

The reaction rate of each reduction step v_m^j, v_w^j and v_{Fe}^j was calculated according to the three-interface model developed by Hara et al. [2] as follows:

$$\begin{aligned} v_m^j = \frac{P}{RT}\frac{4\pi r_0^2}{W_3}[&A_3(A_2+B_2+B_3+F) \\ &+(A_2+B_2)(B_3+F)(Y-Y_{em}^j) \\ &-[A_3(B_2+B_3+F)+B_2(B_3+F)](Y-Y_{ew}^j) \\ &-A_2(B_3+F)(Y-Y_{eFe}^j)], \end{aligned} \qquad (10)$$

$$\begin{aligned} v_w^j = \frac{P}{RT}\frac{4\pi r_0^2}{W_3}[&[(A_1+B_1+B_2(A_3+B_3+F) \\ &+A_3(B_3+F)](Y-Y_{ew}^j)-[B_2(A_3+B_3+F) \\ &+A_3(B_3+F)](Y-Y_{em}^j) \\ &-(A_1+B_1)X(B_3+F)(Y-Y_{eFe}^j)], \end{aligned} \qquad (11)$$

$$\begin{aligned} v_{Fe}^j = \frac{P}{RT}\frac{4\pi r_0^2}{W_3}[&[(A_1+B_1)(A_2+B_2+B_3+F) \\ &+A_2(B_2+B_3+F)](Y-Y_{eFe}^j). \end{aligned} \qquad (12)$$

In these equations the parameters A, B, F and W are given by:

$$A_1^j = \frac{1}{(1-R_m^j)^{2/3}}\frac{1}{k_{cm}^j(1+\frac{1}{K_m^j})}, \qquad (13)$$

$$A_2^j = \frac{1}{(1-R_w^j)^{2/3}}\frac{1}{k_{cw}^j(1+\frac{1}{K_w^j})}, \qquad (14)$$

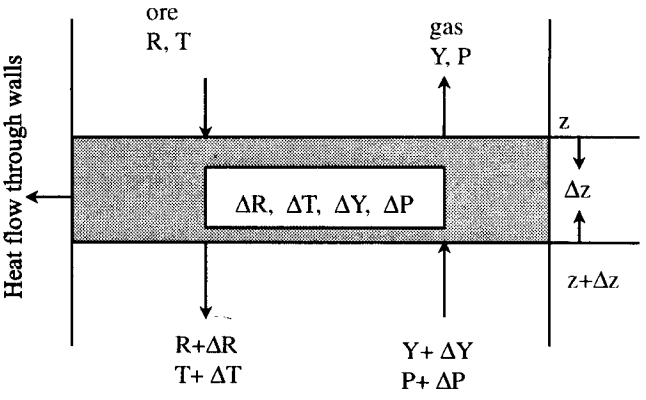

Figure 1. Mass, energy and pressure balances in a volume slice of a HyL III reactor for iron ore reduction

$$A_3^j = \frac{1}{(1-R_{Fe}^j)^{2/3}}\frac{1}{k_{cFe}^j(1+\frac{1}{K_w^j})}, \qquad (15)$$

$$B_1^j = \frac{(1-R_w^j)^{1/3}-(1-R_m^j)^{1/3}}{(1-R_m^j)^{1/3}(1-R_w^j)^{1/3}}, \qquad (16)$$

$$B_2^j = \frac{(1-R_{Fe}^j)^{1/3}-(1-R_w^j)^{1/3}r_0}{(1-R_w^j)^{1/3}D_{eFe}^j}, \qquad (17)$$

$$B_3^j = \frac{1-(1-R_{Fe}^j)^{1/3}r_0}{(1-R_{Fe}^j)^{1/3}D_{eFe}^j}, \qquad (18)$$

$$F^j = 1/k_g^j, \qquad (19)$$

$$\begin{aligned} W_3^j = (A_1^j+B_1^j)[&A_3^j(A_2^j+B_2^j+B_3^j+F^j) \\ &+(A_2^j+B_2^j)(B_3^j+F^j)] \\ &+A_2^j[A_3^j(B_2^j+B_3^j+F^j)+B_2^j(B_3^j+F^j)]. \end{aligned} \qquad (20)$$

A linear addition of the fractional reduction for every mineralogical species (m, w and Fe) is assumed in order to obtain the total reduction , this means:

$$R_m = \Sigma R_m^j,\ R_w = \Sigma R_w^j \text{ and } R_{Fe} = \Sigma R_{Fe}^j. \qquad (21)$$

The heat balance in the bed of solids is given as:

$$\frac{dT_s}{dz} = \frac{6(1-\varepsilon)}{d_p}S\left[h_p(T_g-T_s)+\Sigma[(\Delta H_i)v_i^j)/(\pi d_p^2)\right] X\left[\Sigma\left[W_k\left(c_{pk}-T_s\frac{dc_{pk}}{dT_s}\right)\right]\right]^{-1}. \qquad (22)$$

The heat balance of the gas is:

$$\frac{dT_g}{dz} = \left[\frac{6(1-\varepsilon)}{d_p} h_p S(T_g - T_s) + \pi D_t U(T_g - T_a)\right] X \left[\Sigma\left[G_l\left(c_{gl} + T_g \frac{dc_{gl}}{dT_g}\right)\right]\right]^{-1} . \quad (23)$$

The subscript k in equation (22) refers to the mineral species that form part of a pellet, thus, k varies from 1 to 8 that is; 1: Fe_2O_3, 2: Fe_3O_4, 3: FeO, 4: Fe (a), 5: CaO, 6: SiO_2, 7: Al_2O_3, 8: MgO. The molar flow rates of every mineralogical species were calculated according to their chemical nature of a reducible or not reducible compound.

Table 1. List of symbols

c_{pk}, c_{gl}	molar specific heat of each solid and gas component, J/kmol K
D	diffusion coefficient, m^2/s
D_{ei}	intraparticle effective diffusion coefficient in the product layer, m^2/s
d_{oi}	removable oxygen concentration in the each reduction step, kmol O/kg pellet
d_p	diameter of pellet, m
D_T	inner diameter of shaft furnace, m
G	gas flow rate, m^3(STP)/s
G_l	molar flow rate of a component gas, kmol/s
G_M	gas mass flux, kg/m^2 s
ΔH_i	heat of reaction, J/kmol
h_p	heat transfer coefficient between the solid bed and gas, J/m^2 s K
k_c	rate constant of chemical reaction, m/s
K_e	equilibrium constant for reduction reaction, -
k_g	mass transfer coefficient, m/s
M	molecular weight, kg/kmol
%Met	metallization degree of a pellet, -
P	pressure, MPa
R	gas constant, kJ/kmol K
R_{ch}	chemical reduction ratio $(CO + H_2)/(CO_2)$, volume fractions in %
R_i	reduction degree of each reduction step, -
r_o	pellet radius, m
R_T	overall reduction degree, -
S	cross area of shaft furnace, m^2
T_a, T_g, T_s	temperatures, ambient, gas and solid, respectively, K
U	global heat transfer coefficient, J/m^2 s K
v_i	reduction rate, kmol/s
W	flow rate of pellet, kg/s
W_k	flow rate of each component of pellet, kmol/s
Y_i	molar fraction of each component gas, -
Y_{ie}	equilibrium molar fraction of each component gas, -
z	distance from the top of the furnace, m
ε	voidage of the bed, -
γ_i	porosity of layer, -
ξ_i	labyrinth factor, -
ϕ	particle shape factor, -
ρ_i, ρ_s	density of component and density of pellet respectively, kg/m^3
μ	gas viscosity, kg/m s
subscripts	
h	hematite
m	magnetite
w	wustite
Fe	iron

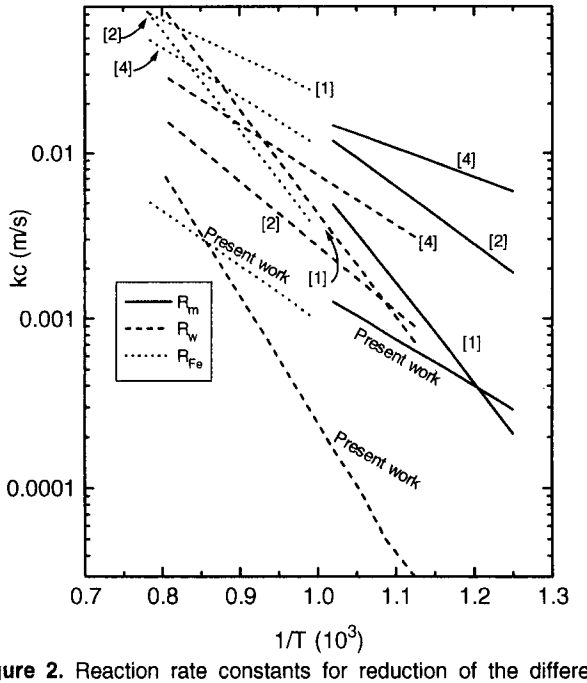

Figure 2. Reaction rate constants for reduction of the different mineralogical species of iron ore employing hydrogen (reactions (1) - (3))

For example, in the first case, $W_1 = (1-R_1)\ (\rho_{Fe_2O_3}/M_{Fe_2O_3})(W/\rho_S)$ and in the fifth one, $W_5 = y_{CaO}\ (\rho_{CaO}/M_{CaO})(W/\rho_S)$. The subscript gl in equation (23) refers to the gaseous species H_2, H_2O, CO and CO_2. Considering the content of oxygen to be removed in each step of reduction, the overall fractional reduction can be calculated through the following expression:

$$R_T = 0.1111 R_m + 0.1889 R_w + 0.700 R_{Fe}. \quad (24)$$

The metallization degree is calculated once that R is

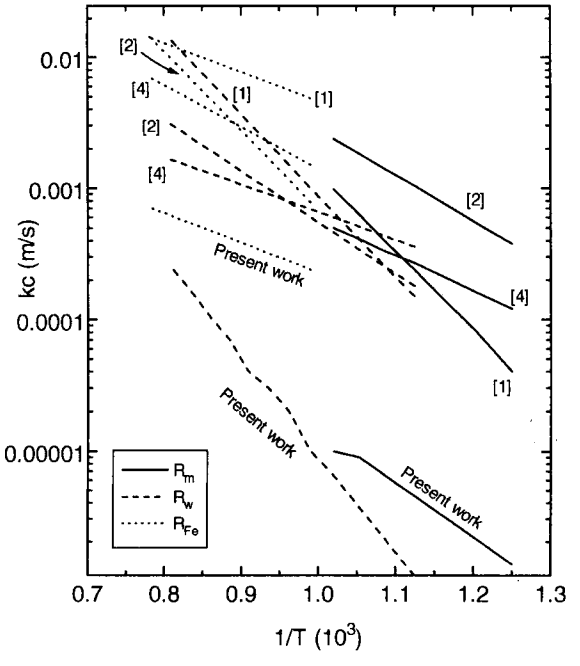

Figure 3. Reaction rate constants for reduction of the different mineralogical species of iron ore employing carbon monoxide (reactions (4) - (6))

known through the following empirical equation obtained from plant data:

$$\%\text{Met} = 150.4R - 50.242. \quad (25)$$

Auxiliary data. The reaction rate constants for every reduction step with H_2 and CO are presented in **figures 2 and 3,** respectively. It is evident from these figures that there are considerable discrepancies in the experimental values for these, supposedly, intrinsic reaction rate constants. In view of this situation the selected constants in the model were those that best fitted the industrial results reported in [5] as will be explained later on. Equilibrium constants for the chemical reactions (1) - (6) were taken from Kubaschewski-Alcock [6]. **Table 2** summarizes the reaction rate and equilibrium constants used in the present model.

Effective diffusivities of reducing gases in the different mineralogical species were calculated through the expression:

$$D_e^j = D^j \gamma_i \xi_i. \quad (26)$$

The labyrinth factors ξi, for H_2-H_2O and CO-CO_2 mixtures employed in the model and the respective porosities, γi, in every mineralogical species as functions of the initial porosity of hematite are reported in table 2. Molecular diffusivities of H_2 and CO as well as viscosities in the multicomponent gaseous phase were calculated using the methods proposed in Bird's et al. book [7]. Thermophysical properties for the solid and gaseous species such as heat capacities were consulted in Geiger's book [8] and they were fitted through polynomial expressions as functions of temperature.

The heat transfer coefficient, h_p, in the countercurrent moving bed was estimated through the following correlation [9]:

$$Nu = 2.0 + 0.39 Pr^{1/3} Re_p^{1/2}. \quad (27)$$

The global heat transfer coefficient, U, employed for the reactor's wall was that reported in reference [3]. On the other hand, the pressure drop along the length of the reactor was calculated through a modification of the Ergun's equation [10] given by:

$$\int_0^z [C_1 \mu G_M + C_2 G_M^2] dz = -\int_0^z P dP, \quad (28)$$

where C_1 and C_2 are expressed as:

$$C_1 = \frac{150(1-\varepsilon)}{\varepsilon^3 (\phi d_p)^2} \quad (29)$$

and

$$C_2 = \frac{1.75(1-\varepsilon)}{\varepsilon^3 \phi d_p}. \quad (30)$$

In these equations an ideal behaviour for the gas phase is implicit. This simplification is valid in the range of pressures usually employed for these reactors.

Numerical method

Equations (7) - (9), (22) - (23) and the auxiliary equations (10) - (20) and (24) - (30) complete the mathematical model for this process. Hara et al. [2] and Yanagiya et al. [1] fed their experimental temperatures and solved the equations (7) - (9) with auxiliary equations (10) - (20) using a Runge-Kutta method. Meanwhile Kaneko et al. [3] and Takahashi et al. [4] claimed that they were able to solve the full model (including the energy balance given by the equations (22) - (23) using a Runge-Kutta-Gill and Runge-Kutta of fourth order methods, respectively. In the present case we were unable to solve the full system of ordinary differential equations using those methods since it presented a very high stiffness. Consequently, the following procedure was employed:

- the Jacobean matrix of the ordinary differential equations (7) - (9) and (22) - (23) was firstly calculated. If the smallest element in this matrix was smaller by an order of magnitude than the maximum element found we proceeded to employ a variable step size method;

Table 2. Reaction rate and equilibrium constants for the model

Step → / gas ↓	$Fe_2O_3 \rightarrow Fe_3O_4$	$Fe_3O_4 \rightarrow FeO$	$FeO \rightarrow Fe$
H_2	$k_c = 0.01\exp(4.49-53.44\times10^3/RT)$ $K_e = \exp(10.32+362.3/T)$	$k_c = 1.0\exp(8.971-143.8\times10^3/RT)$ $K_e = \exp(8.454-7910.6/T)$	$k_c = 0.5\exp(1.381-63.36\times10^3/RT)$ $K_e = \exp(0.930-1585.0/T)$
CO	$k_c = 0.01\exp(3.16-80.32\times10^3/RT)$ $K_e = \exp(7.255+3720.0/T)$	$k_c = 0.038\exp(8.971-143.8\times10^3/RT)$ $K_e = \exp(5.289-4711.0/T)$	$k_c = 0.01\exp(1.381-42.81\times10^3/RT)$ $K_e = \exp(-3.127+2879/T)$

Table 3. Labyrinth factors and porosities for the mineralogical species employed in the model

Step → / gas ↓	$Fe_2O_3 \rightarrow Fe_3O_4$	$Fe_3O_4 \rightarrow FeO$	$FeO \rightarrow Fe$
[12]	$\gamma_m = \gamma_h + 0.022A(1-\gamma_h)$	$\gamma_w = \gamma_h + 0.165A(1-\gamma_h)$	$\gamma_{Fe} = \gamma_h + 0.533A(1-\gamma_h)$
H_2-H_2O	$\log_{10}\xi = 0.382\times10^{-2}T-4.954$	$\log_{10}\xi = 0.159\times10^{-2}T-2.069$	$\xi = 0.491\times10^{-3}T-0.222$
CO-CO_2	$\log_{10}\xi = 0.382\times10^{-2}T-5.352$	$\log_{10}\xi = 0.159\times10^{-2}T-2.467$	$\log_{10}\xi = 0.124\times10^{-2}T-1.734$ ($T \geq 1173$ K) $\log_{10}\xi = 0.102\times10^{-1}T-12.25$ ($T < 1173$ K)

$$A = \frac{(\%Fe_2O_3)\cdot r_s}{100\cdot r_{Fe_2O_3}}$$

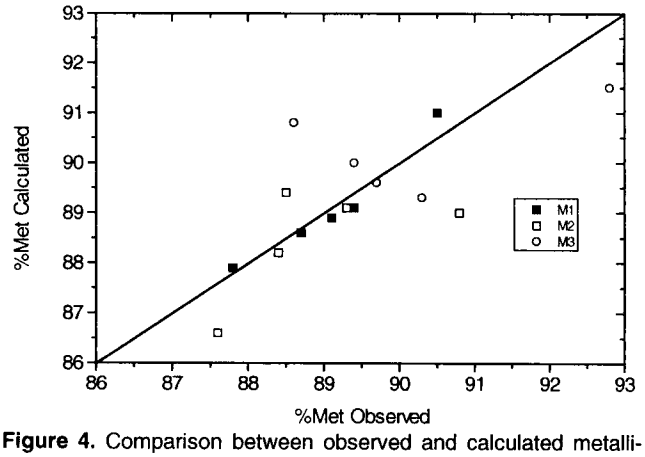

Figure 4. Comparison between observed and calculated metallization of DRI for the three feed mixtures

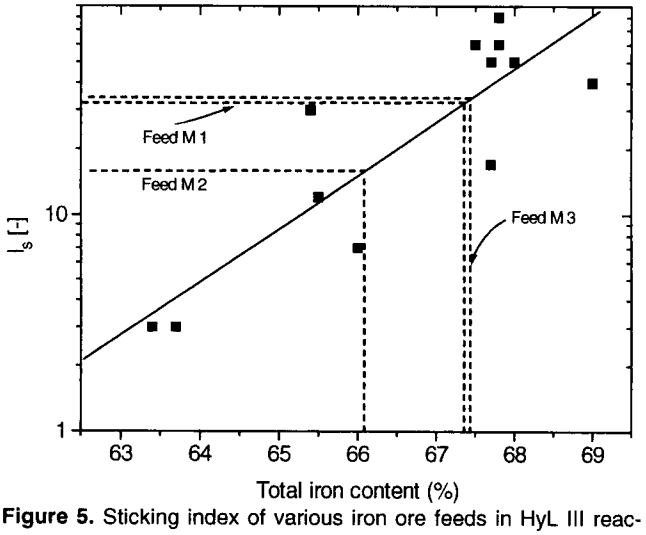

Figure 5. Sticking index of various iron ore feeds in HyL III reactors

Table 4. Conditions of reducing gas in the reactor

Temperature, K			G	W	W/G	volume fraction of reducing gas, V, in %				
T_I	T_{RR}	T_{ER}	m³(STP)/s	kg/s	kg/m³(STP)	H_2	CO	CO_2	CH_4	N_2
mixture 1										
	828	426	37.39	18.48	0.494	61.86	20.51	11.80	4.04	1.79
910	829	426	37.53	19.45	0.518	61.87	20.68	12.00	4.62	0.83
	830	427	37.46	19.39	0.517	61.00	20.60	11.80	4.70	1.90
	831	442	37.47	18.58	0.496	61.90	19.89	11.20	5.60	1.41
911	827	424	37.45	19.69	0.526	62.40	19.91	11.72	4.68	1.29
mixture 2										
909	831	415	37.13	18.77	0.506	59.01	21.88	12.68	3.76	2.67
907	833	441	34.74	16.75	0.482	61.05	20.86	12.00	4.52	1.57
911	831	432	37.54	18.87	0.503	62.07	20.48	11.60	4.05	1.80
877	820	412	33.99	17.31	0.509	61.60	19.94	12.68	4.34	1.44
906	828	408	36.15	19.11	0.528	61.22	21.02	12.32	4.39	1.05
mixture 3										
908	837	456	40.09	20.14	0.503	60.41	19.25	12.11	4.94	3.29
904	822	456	40.10	18.91	0.472	60.82	19.40	12.20	5.95	1.63
905	828	461	39.82	20.63	0.518	60.28	18.99	12.22	6.01	2.50
904	823	444	37.24	19.26	0.517	60.52	19.14	12.54	5.60	2.20
	827	455	40.07	20.88	0.521	60.50	20.86	12.00	5.47	1.17

– if the system resulted in high stiffness, according to the criterion mentioned above, a variable step-size, variable order backward differentiation method was used. This model was solved in a personal computer of the Process Metallurgy Group at IPN-ESIQIE.

Results and discussion

Figures 2 and 3 report the chemical rate constants for the reactions (1) - (3) and (4) - (6) for hydrogen and carbon monoxide, respectively, from various experimental sources. As can be seen, there is a great data spread out for both kinds of reducing gases. Owing to this dispersion it was decided to employ these reaction rate constants as fitted parameters of the present model. For this reason the model was run under various operating conditions and the final values for these constants were those that yielded the best fit to the experimental observations regarding temperature, chemical composition of gases and final metallization degree of DRI. These fitted parameters are also indicated in figures 2 and 3 and reported in **table 3.** In order to test the accuracy of this approach mathematical simulations were performed for the reduction kinetics for the three ore mixtures (feed mixtures) reported in another paper [5], running the reactor under the operating conditions shown in **table 4.** Here it should be mentioned that since the feed mixture 2 showed low sensitivity to changes on the operating conditions the diffusivities of H_2 and CO in the ash layer were decreased to half the value calculated by equation (26) during the last reduction step.

The results are presented in **figure 4** for the final metallization degree of DRI and the excellent agreement between the calculated values by the present mathematical model and those observed during actual operation of the plant in the case of feed mixture 1 is evident. Some dispersion is observed between both kinds of values for mixture 2 owing to the low sensitivity of this mixture to the operating parameters of the reactor as has been already mentioned in [5]. However, the mathematical predictions are acceptably accurate.

In the case of feed mixture 3 the differences between predicted and observed values are considerably larger. This coincides with the fact that this feed always presented frequent problems of cluster formation inside the reactors [5].

In this regard the sticking index [11] is a mechanical test that allows the measurement of the resistance of a cluster and in some sense also the tendency to clustering of a given ore. This index is given by:

$$I_s = \frac{(\omega_I + \omega_{20})/2 + \sum \omega_i}{\frac{20}{\omega_I}}, \qquad (31)$$

where I_S is the sticking index, ω_I is the cluster's weight before the tumbling test, ω_{20} is the cluster weight after the 20^{th} test and ω_i is the weight after the test i. This index is plotted against the total content of iron in a given ore and the experimental data are presented in **figure 5.** Since the feed mixture 3 has the highest iron content (table 2 of reference [5]) one can expect a higher tendency to formation of clusters. This increase in the tendency to cluster together with the increase in the total iron content in a reactor's charge is assumed to take place due the nucleation of iron whiskers in the outer layer of pellets. The weight of the charge presses the pellets against each other promoting their joining just near the inlet of reducing gas, where the temperature is at its highest. This joining phenomenon between pellets is facilitated by the presence of the iron whiskers located on their outer layers.

Consequently, these differences in DRI metallization in this feed mixture must have their origin in fluid flow malfunctions, influenced by the presence of clusters, directly affecting the gas-solid contact and modifying the dynamic response of the system.

Coming back to the results of feed mixture 2 and in order to perform a more detailed analysis, **figure 6** shows additional simulation results: in the case of increasing the reducing power of incoming gases the reduction rate for the transformations from hematite to magnetite and from magnetite to wustite also increases but the rate levels off when the transformation of wustite to iron is taking place. Thus, the final metallization degree will, in practical terms, be independent of the reducing power of gases and, to some extent, of the solid-gas contact which can be defined simply as the ratio of mass flow of solids/mass flow of gases. A sound explanation of this phenomenon is, at the moment, not within the objectives of the present work, however, it is known that this mixture contains Sidor pellets which have a high lime concentration (see table 2 of reference [5]) and it is probable that this lime is able to partially flux the gangue forming a liquid that clogs the pores similarly to the experimental observations reported by Kaneko et al. [3].

Figures 7a-c show the simulation profiles of temperature, reduction of every transformation in the three interface kinetics, total reduction degree and metallization of DRI along the length of the reactor for the three types of feed.

Feed mixture 3 reaches higher metallizations than feed mixtures 1 and 2 while the latter observes a levelling off, as already mentioned, at the top of the reactor being unable to reach metallizations higher than 90%. Another interesting aspect is that the reaction rate from the reduction from hematite to magnetite is very fast particularly for the feed mixture 3. Regarding the other reduction reactions from magnetite to wustite and from wustite to iron they start from the top of the reactor and 4 m, approximately, below this reference point, respectively, and both come to an end just in the lowest part of the reactor. It is the last quarter of the reactor's length where the most important contribution to the total reduction takes place.

The profiles for the chemical composition of the gaseous phase along the length of the reactor are shown in **figures**

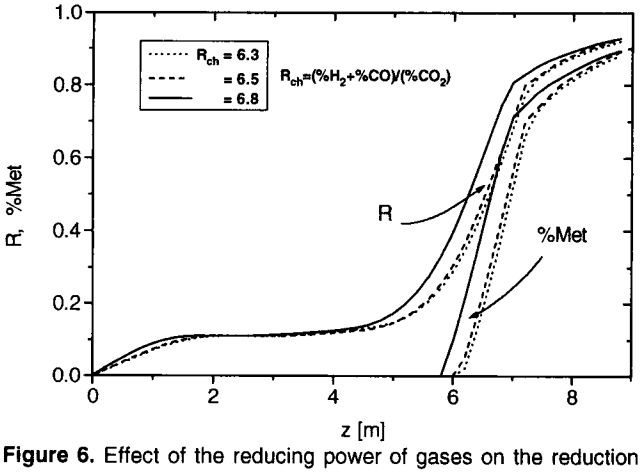

Figure 6. Effect of the reducing power of gases on the reduction degree and metallization of DRI in HyL III reactor for feed mixture 2

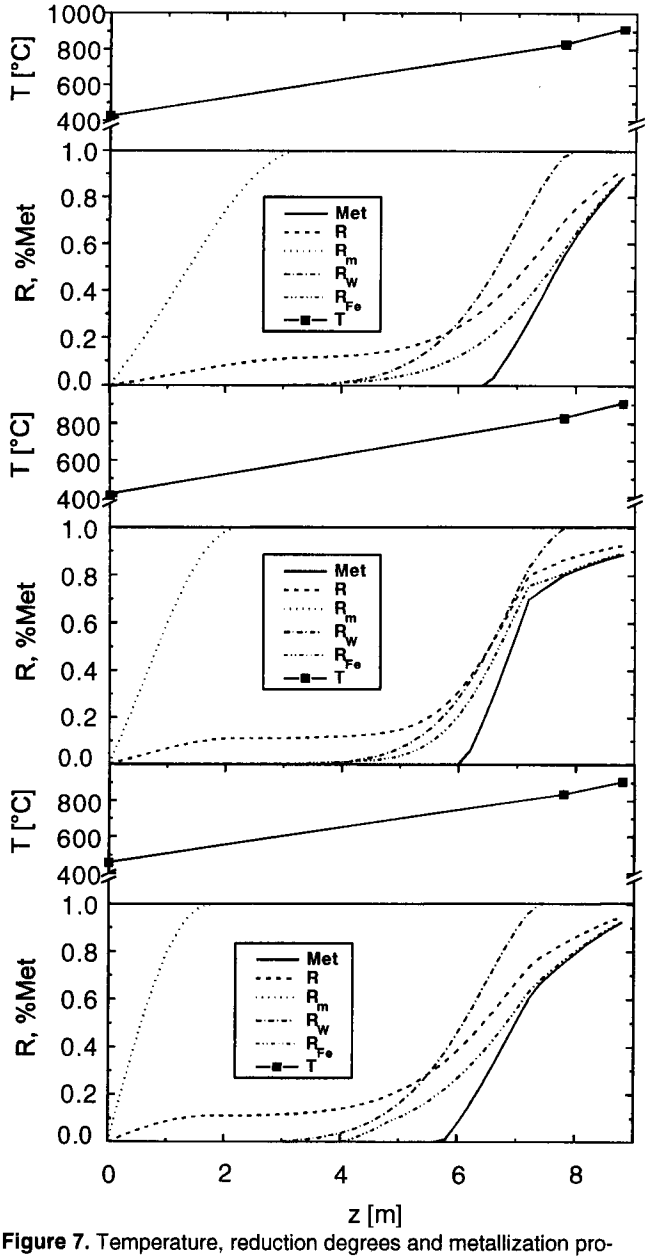

Figure 7. Temperature, reduction degrees and metallization profiles along the length of HyL III reactors

8a-c for the feed mixtures 1, 2 and 3 respectively. Here it can be observed that carbon monoxide reacts to a very small extent and these predictions are in quite good agreement with the chemical analysis of gaseous samples taken in the inlet and outlet ducts of the reactor. According to the experimental measurements and the mathematical predictions the reduction degree of these feed mixtures is essentially controlled by the reducing power of hydrogen.

Under the present status this mathematical simulator is reliable enough to simulate the reduction rate of these mixtures running the DRI plant under different operating conditions. Eventually it can be modified to simulate any other feed mixtures by carrying out a calibration like the one employed in this work, either using the reaction rate constants as fitted parameters or diffusivities of gaseous species in the ash layer at the last reduction step.

To explain the high dispersions between observed and calculated plant data for feed mixture 3, fluid flow modifications due to heterogeneous flow of solids should be taken into account. This will, surely, lead to substantial variations of metallization of DRI through the reactor's diameter at the lowest part the reactor.

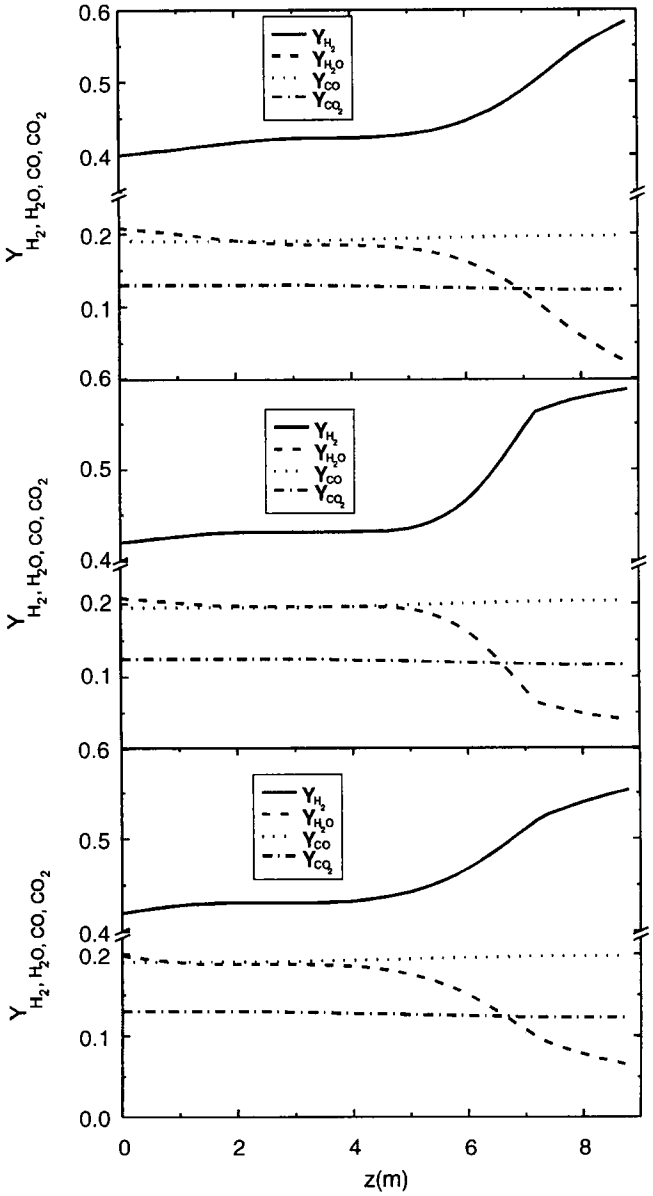

Figure 8. Chemical composition profile of the gaseous phase along the length of HyL III reactors

Conclusions

Heat transfer and chemical reaction models of iron ore reduction in countercurrent moving bed reactors have been built and tested in comparison to industrial results of a currently operating HyL III reactor and the main conclusions reached in this work are as follows:

- the models predict very well the metallization degree and thermal profiles of feed mixture 1 and losses accuracy with feed mixtures 2 and 3;
- feed mixture 2 reported low sensitivity to changes in the operating parameters of the reactor and this can be explained only by a decrease in the diffusivity of the reducing gases through the ash layer. When this factor is introduced into the reaction model the simulator is able to explain this low sensitivity of this feed mixture to the reducing conditions;
- industrial measurements reported that the carbon monoxide plays a minor role on the reduction rate of these three feed mixtures and this behaviour is also predicted by the models described here;
- high dispersion observed between the observed and predicted data for the feed mixture 3 should have its origin in problems related with the gas-solid contact efficiency, fluid flow malfunctions should lead to this condition. The plant observations indicate that, indeed, this mixture always reported a higher tendency to cluster formation inside the reactors. This situation leads to the need of a 3D simulator, a task that the authors are currently undertaking.

(A 01 313; received: 05. June 1997)

References

[1] *Yanagiya, T.; Yagi, T.; Omori, Y.:* Ironmak. Steelmak. (1979) No. 3, p. 93/100.

[2] *Hara, Y.; Sakawa, M.; Kondo, S.:* Tetsu-to-Hagané 62 (1976) No. 3, p. 315/23.

[3] *Kaneko, D.; Takenaka, Y.; Kimura, Y.; Narita K.:* Trans. ISIJ 22 (1982), p. 88/97.

[4] *Takahashi, R.; Koyabu, Y.; Ishii, M.; Ishigaki, M.; Takahashi, Y.:* Tetsu-to-Hagané 66 (1980) No. 13, p. 1985/94.

[5] *Garnica-González, P.; Morales, R. D.; Sosa, R.:* to be published.

[6] *Kubaschewski, O.; Alcock, C. B.:* Metallurgical Thermochemistry, 5th edn., Pergamon Press, New York, 1979.

[7] *Bird, R. B.; Stewart, W.E.; Lightfoot, E.N.:* Transport Phenomena, Wiley Intern., New York, 1960, p. 3/30; 243/62;495/516.

[8] *Poirier, D.R.; Geiger, G.H.:* Transport Phenomena in Materials Processing, TMS, Pennsylvania, 1994.

[9] *Akiyama, T.; Takahashi, R.; Yagi, J.:* ISIJ Intern. 31 (1994) No. 1, p. 24/31.

[10] *Wonchala, E.P.; Wynnyckyj, J.R.:* Met. Trans. 18B (1987), p. 279/80.

[11] Curso Nacional de Siderurgia, Instituto Tecnológico de Morelia, México, 1996.

[12] *Ohmi, M.; Naito, M.; Usui, T.:* Tetsu-to-Hagané 69 (1983) No. 6, p. 546/55.